Isolating the Charge-Transfer Component of the Anionic H Bond Via Spin Suppression of the Intracluster Proton Transfer Reaction in the $NO^-\cdot H_2O$ Entrance Channel Complex†

William H. Robertson and Mark A. Johnson*

Sterling Chemistry Laboratory, Yale University, P.O. Box 208107, New Haven, Connecticut 06520

Evgeniy M. Myshakin and Kenneth D. Jordan*

Department of Chemistry and Center for Molecular and Materials Simulations, University of Pittsburgh, Pittsburgh, Pennsylvania 15260

Received: April 3, 2002; In Final Form: June 25, 2002

We report the vibrational predissociation spectrum of the $NO^-\cdot H_2O$ complex in the OH stretching region. The ionic H-bonded OH stretch is much less red-shifted and less structured in the vibrational spectrum of $NO^-\cdot H_2O$ than in that of the $O_2^-\cdot H_2O$ cluster, despite the larger proton affinity of NO^- relative to O_2^-. It is argued that the differences between the spectra of these two species are primarily a consequence of the greater charge-transfer character in the $O_2^-\cdot H_2O$ cluster and that the charge-transfer component is much less important in $NO^-\cdot H_2O$ because of its triplet spin character.

Introduction

In a recent series of papers,[1−8] we have used infrared spectroscopy to quantify how a water molecule is distorted upon attachment to the spherical halide ions[1−6] as well as to structured molecular anions such as superoxide, O_2^-.[7,8] In all of these systems, the water molecule attaches to the ion in an asymmetric arrangement in which one hydrogen is engaged in a strong hydrogen bond to the ion with the other free. The stretching frequency of the ionic H-bonded OH stretch (OH_{IHB}) was found to shift dramatically to lower energy in a systematic way according to the basicity of the anion. Recently, Thompson and Hynes[9] have analyzed the origin of this trend using a valence-bond model and have concluded that the shifts have both electrostatic and intracluster charge-transfer (CT) contributions, with the importance of the latter becoming more pronounced in the more strongly bound systems. For weak bases such as the halide anions (X^-), the CT component may be viewed as arising from mixing between the diabatic $X^-\cdot H_2O$ ground and $XH\cdot OH^-$ excited states. Thus, one would expect the CT contribution to the wave function to grow in importance with increasing proton affinity of the anion because the energy separation between the two diabatic configurations should decrease with increasing proton affinity as the basicity of X^- approaches that of OH^-.

In this paper, we explore the charge-transfer model of the intramolecular OH stretch red shift by comparing the vibrational spectrum of the $NO^-\cdot H_2O$ cluster with those measured previously for the $O_2^-\cdot H_2O$ and halide−water complexes.[2,7,8] If only electrostatic interactions were important, one would expect comparable OH_{IHB} red shifts for $NO^-\cdot H_2O$ and $O_2^-\cdot H_2O$. Because the proton affinity of NO^- is greater than that of O_2^- (1511.7 ± 0.84 vs 1477.0 ± 2.9 kJ/mol[10]), one might expect charge transfer to be of even greater importance for $NO^-\cdot H_2O$ than for $O_2^-\cdot H_2O$. However, as Brauman and co-workers[11,12] have pointed out, the lowest-energy proton transfer for NO^-,

$$NO^-(^3\Sigma) + H_2O(^1A_1) \rightarrow HNO(^1A') + OH^-(^1\Sigma) \quad (1)$$

is spin-forbidden, whereas that for O_2^- is allowed because this species has $^2\Pi_g$ ground-state symmetry and yields $^2A''$ HO_2 proton-transfer products. Consequently, in assessing the role of charge transfer (CT) in the $NO^-\cdot H_2O$ complex, one should instead consider the reaction to give $HNO(^3A'') + OH^-(^1\Sigma)$, which lies 205 kJ/mol higher in energy than the singlet proton-transfer products.[13] (Actually, this is the relevant reaction if the water molecule is bound on the N atom of NO^-. If it is bound to the O atom, then the appropriate reaction is that to give $HON(^3A'') + OH^-(^1\Sigma)$, which, as discussed below, lies even higher in energy.) As a result, it is anticipated that CT actually plays less of a role in $NO^-\cdot H_2O$ than in $O_2^-\cdot H_2O$ and that this spin suppression of the CT process provides a way to isolate and evaluate electrostatic effects on H-bond red shifts experimentally. This will be used to assess the relative contributions of CT and electrostatics to the large red shift observed in the $O_2^-\cdot H_2O$ complex.

Experimental Section

Spectra were obtained using argon predissociation spectroscopy,

$$NO^-\cdot H_2O\cdot Ar_n + h\nu \rightarrow NO^-\cdot H_2O\cdot Ar_m + (n-m)Ar \quad (2)$$

with $n = 1-11$ to determine which bands are sensitive to the extent of argon solvation. Upon excitation at 2950 cm^{-1}, the $NO^-\cdot H_2O\cdot Ar_{11}$ complex displays a mean argon loss of 4.4 atoms, implying an effective binding energy of 670 cm^{-1}/Ar. Briefly, this was accomplished with the Yale tandem time-of-flight photofragmentation apparatus, which features cluster ion formation via controlled reactions in an electron beam ionized, pulsed supersonic expansion.[14] Neutral reagents were introduced just outside the nozzle at low pressure by pulsed injection into the pure argon supersonic expansion.[15] In the $NO^-\cdot H_2O\cdot Ar_n$ case of interest here, $(H_2O)_{2,3}^-\cdot Ar_n$ clusters were first generated

† Part of the special issue "Jack Beauchamp Festschrift".

* Corresponding author. E-mail: mark.johnson@yale.edu.

10.1021/jp020891s CCC: $22.00
Published on Web 08/21/2002

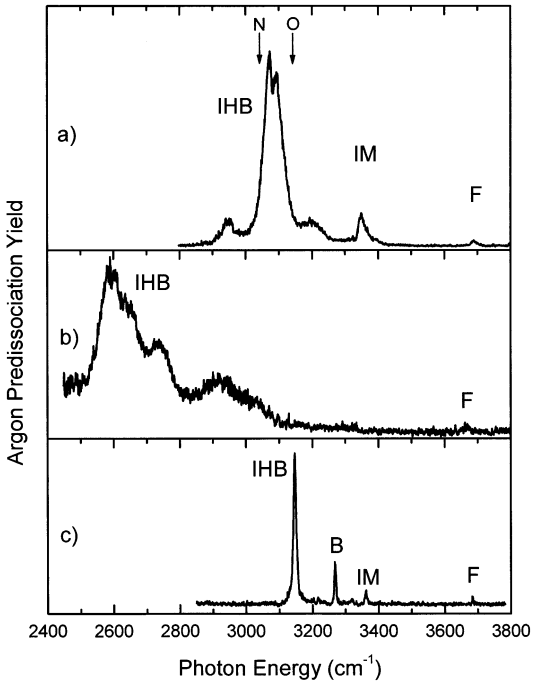

Figure 1. OH stretching spectra obtained by argon predissociation: (a) $NO^-\cdot H_2O\cdot Ar_4$, (b) $O_2^-\cdot H_2O\cdot Ar_3$ from ref 7, and (c) $Cl^-\cdot H_2O\cdot Ar_{11}$ from ref 20. Despite the greater proton affinity of NO^- compared to that of O_2^-, the OH_{IHB} red shift is much smaller for $NO^-\cdot H_2O$ than for $O_2^-\cdot H_2O$. Assignments are IHB for ionic H-bonded OH stretch, B for intramolecular bend overtone, IM for ion−molecule stretch combination band, and F for free-OH stretch. Arrows in panel (a) indicate the OH_{IHB} stretching fundamentals calculated at the UMP2/aug-cc-pVTZ level with a 0.956 scale factor for the two $^3NO^-\cdot H_2O$ isomers (i.e., with the water H-bonded to the N or the O, respectively).

by the introduction of water vapor, followed by a trace amount of NO brought in through a third pulsed valve. The mass-selected $NO^-\cdot H_2O\cdot Ar_n$ ions were excited with the output from a KTP/KTA optical parametric oscillator/amplifier (Laser Vision) pumped by a Nd/YAG laser (Quanta Ray DCR3). Fragment ions were separated with a second mass filter (reflectron) and collected with a boxcar averager while the laser was scanned through the 2400−4000 cm^{-1} region. The reported spectra arise from the addition of typically 20−30 individual scans and are normalized to correct for laser output energy fluctuations. Laser pulse energies were in the range of 2−4 mJ/pulse with a bandwidth of about 2 cm^{-1}.

Results and Discussion

The vibrational spectrum of $NO^-\cdot H_2O\cdot Ar_4$ in the OH stretch region is shown in Figure 1 along with the spectra of $O_2^-\cdot H_2O\cdot Ar_3$ and $Cl^-\cdot H_2O\cdot Ar_{11}$ for comparison. The vibrational spectra of all three clusters display a weak, sharp feature near 3700 cm^{-1}, the signature of a free OH group, which indicates that the water molecule is attached to the ion in an asymmetric, single H-bond motif. All three complexes display much more oscillator strength at the low-energy end of the spectrum, characteristic of an anionic H-bonded OH stretching vibration (OH_{IHB}). The low-frequency bands in $O_2^-\cdot H_2O$ are very broad, extending from 2400 to 3200 cm^{-1}, whereas the corresponding structure in the $NO^-\cdot H_2O$ spectrum is much sharper, with a dominant band at 3070 cm^{-1} (Figure 1a, IHB) and a weaker companion band (IM) toward higher energy at 3360 cm^{-1}. There is also structure near 2950 and 3200 cm^{-1} flanking the main band, with both of these weak bands being incrementally enhanced with an increasing number of attached argon atoms,

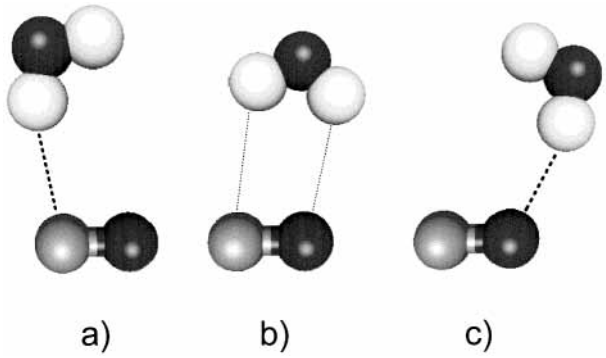

Figure 2. Geometrical structures of $^3NO^-\cdot H_2O$ optimized at the UMP2/aug-cc-pVDZ level showing the (a) H-bond to nitrogen, (b) transition state, and (c) H-bond to oxygen (global minimum).

leading us to attribute them to a less-populated isomer (further discussed below) with associated combination band structure.

In light of the relative simplicity of the vibrational spectrum of $NO^-\cdot H_2O$ and its similarity to that observed for $Cl^-\cdot H_2O$, we assign the 3070 cm^{-1} band in $NO^-\cdot H_2O$ to the OH_{IHB} in an asymmetric complex and the much smaller band at 3698 cm^{-1} to the associated free OH group. The weaker band near 3360 cm^{-1} can arise from an ion−molecule stretching vibration in combination with the OH_{IHB} or the bending overtone. Such bands are also observed in the spectra of halide−water complexes with similar spacings (see Figure 1c and ref 2).

Of course, the $NO^-\cdot H_2O$ complex has the added complication (compared to the Cl^- and O_2^- hydrates) that there are likely two isomeric forms depending on whether the ionic H-bond is directed toward the nitrogen or the oxygen atom. If only electrostatic interactions were important, one might expect that the hydrogen would prefer to bind to the site with the greater excess charge density, which chemical intuition would indicate lies on the oxygen atom. To explore the isomer issue, geometry optimizations were carried out at the MP2/aug-cc-pVDZ[16,17] level of theory.[18] Stationary points were recovered corresponding to the two expected isomers as well as the transition state for their interconversion. The optimized structures are depicted in Figure 2. Single-point CCSD(T)/aug-cc-pVTZ[16,17] calculations carried out at the MP2/aug-cc-pVDZ optimized geometries predict the O-bound isomer to be more stable by about 240 cm^{-1} and the barrier for isomerization from the N-bound to the O-bound complex to be very small (∼30 cm^{-1}). The calculations also predict the red shift of the OH_{IHB} to be about 100 cm^{-1} greater in the N-bound than in the O-bound isomer. The scaled harmonic frequencies (0.956 scaling factor) calculated at the MP2/aug-cc-pVTZ level are indicated by the arrows in Figure 1.

The evolution of the $NO^-\cdot H_2O$ bands with argon solvation (shown in Figure 3) supports the assignment of the bands to two low-energy isomers where the relative populations change with the number of attached argon atoms. Whereas the band positions only slightly blue shift with added argon atoms, the weak 2950 cm^{-1} band in the $NO^-\cdot H_2O\cdot Ar$ spectrum is dramatically enhanced with increasing solvation, and the initially dominant 3070 cm^{-1} band is suppressed. Because the theoretical results place the OH_{IHB} band associated with the N-bound isomer ∼100 cm^{-1} below that of the O-bound isomer, we assign the 2950 cm^{-1} band to the OH_{IHB} of the N-bound isomer. The weaker 3200 cm^{-1} band tracks the 2950 cm^{-1} band's argon-dependent intensity and blue shift and therefore is assigned to the ion−molecule stretch combination band of the N-bound isomer (bracket in Figure 3a). The 3070 cm^{-1} band is then traced to the OH_{IHB} of the O-bound isomer. Finally, we note that the

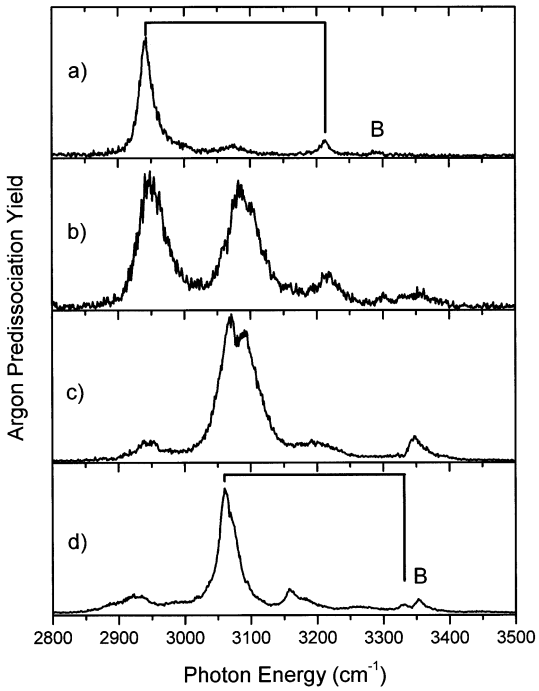

Figure 3. Argon solvation dependence of the $^3NO^-\cdot H_2O$ predissociation spectra: (a) $^3NO^-\cdot H_2O\cdot Ar_{11}$, (b) $^3NO^-\cdot H_2O\cdot Ar_8$, (c) $^3NO^-\cdot H_2O\cdot Ar_4$, and (d) $^3NO^-\cdot H_2O\cdot Ar_1$. B indicates the overtone transition of the intramolecular water bending mode, and IM denotes the ion−molecule stretch combination band built on the OH_{IHB}. Each bracket connects a given OH_{IHB} band with its ion−molecule combination band. Traces a, c, and d show total photofragment ion yield whereas trace b displays only the production of the $NO^-\cdot H_2O\cdot Ar_3$ fragment.

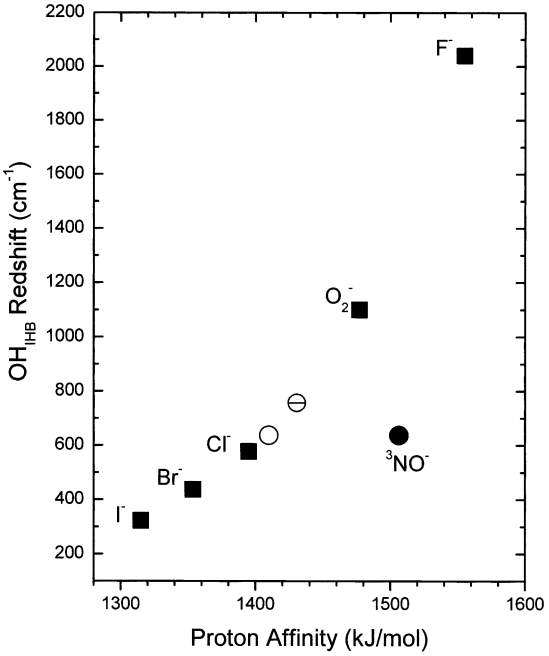

Figure 4. Red shift of the H-bonded OH stretch fundamental as a function of ion proton affinity for H_2O complexed to various negative ions. Note the deviation of NO^- (●) from the trend of the other ions (■) due to the spin-forbidden nature of the lowest-energy proton-transfer reaction. The open circle (○) designates the O-bound isomer with the proton affinity of NO^- corrected to account for the formation of triplet HON (see text and eq 3). The dashed circle (⊖) shows the OH_{IHB} red shift for the N-bound isomer plotted with the spin-corrected PA. Red shifts are taken from this work and refs 2, 4, 7, and 22; the proton affinities are from ref 10.

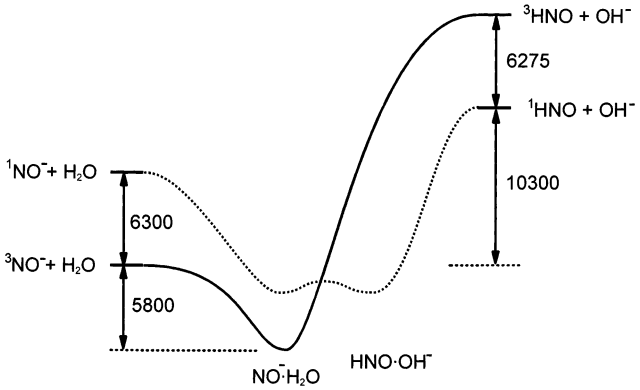

Figure 5. Energy-level schematic for the $NO^- + H_2O$ proton-transfer reaction. Note that reaction between the lowest product and reactant states is spin-forbidden. Asymptotic energies (cm^{-1}) and the well depth on the triplet surface (solid line for the $HNO(^3A'') + OH^-(^1\Sigma)$ products) are taken from experiment.[10,13,23−27] The double-well nature of the singlet excited-state surface, shown schematically here (- - -), is recovered in CASSCF calculations.

3070 cm^{-1} band is accompanied by a second peak at 3090 cm^{-1} in the complex with four Ar atoms (Figure 3c). We believe that this doublet structure is a consequence of isomers based on different arrangements of the Ar atoms around the O-bound form of the core complex.[19,20]

Regarding the assignment of the weaker features, the doublet near 3350 cm^{-1} (Figure 3d) is assigned to the ion−molecule combination band of the O-bound isomer and the overtone of the intramolecular bend of the water molecule. Note that in this scheme the bend overtone red shifts but the OH_{IHB} blue shifts with increasing solvation, consistent with the trends observed in the halide−water and $Cl^-\cdot H_2O\cdot(CCl_4)_n$ spectra.[2,6] Because the N-bound isomer is calculated to have a very shallow minimum, it is possible that this "isomer" is actually explored by soft-mode vibrational excitation of the O-bound form and that the spectral changes reflect subtle changes in the potential for the high-amplitude motion.[21] It is important to emphasize, however, that despite the complication introduced by the isomers the structure associated with the OH_{IHB} stretch in the $NO^-\cdot H_2O$ spectrum is much simpler and less red-shifted than that in the spectrum of superoxide hydrate.

In Figure 4, we plot the observed OH_{IHB} red shift[2,4,7,22] as a function of proton affinity[10] (PA) for water complexed to a number of anions. With the exception of $NO^-\cdot H_2O$, the data (■) fall on a monotonic curve. The OH_{IHB} red shift of the dominant OH_{IHB} band (3070 cm^{-1}) arising from $NO^-\cdot H_2O$ (●) is much smaller than expected on the basis of the thermodynamic proton affinity of NO^- (eq 1) and the general trend depicted in Figure 4. However, if the intracluster proton-transfer reactions that govern the CT contributions are confined to the triplet surface, the relevant proton affinity is reduced according to the promotion energy required to form triplet products (see Figure 5). Moreover, to the extent that the complexes are frozen into a particular isomeric (N-bound or O-bound) form, there is an additional complication due to the necessity to invoke site-specific proton affinities.[28] This arises because the N-bound form leads to ^3HNO formation whereas the O-bound form correlates to the ^3HON isomer.

To refine the shift versus PA behavior to account for site specificity and spin conservation, one needs to identify the origin band from a particular isomer and plot the associated shift as a function of the PA corresponding to formation of the appropriate triplet isomer of HNO. In the case of the N-bound isomer, the OH_{IHB} origin was assigned above to the 2950 cm^{-1} band (757 cm^{-1} shift), whereas the PA correction requires the energy

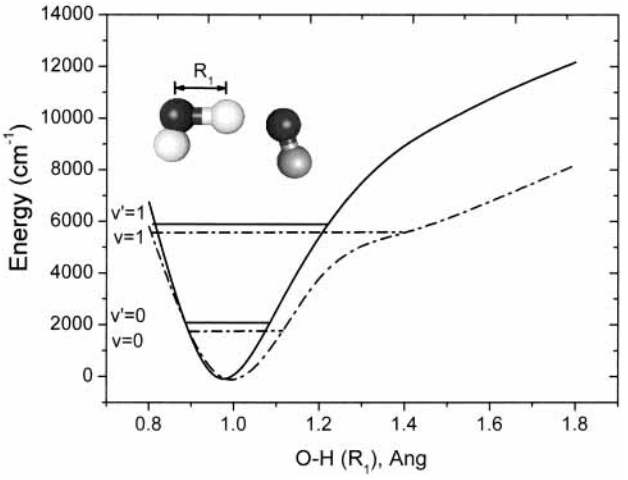

Figure 6. CASSCF/aug-cc-pVDZ potential energy curves governing the motion of the proton between the O atom of the water and an O atom of O_2^- (− - −) or the N atom of NO^- (—). The CASSCF(5,4) and CASSCF(8,6) procedures were used for $O_2^-\cdot H_2O$ and $NO^-\cdot H_2O$, respectively. To illustrate the extreme nature of the anharmonicity, the energies of the $\upsilon = 0$ and 1 harmonic vibrational levels are indicated by horizontal lines. Note that the potential energy curve for $O_2^-\cdot H_2O$ displays much stronger anharmonicity than does $^3NO^-\cdot H_2O$, especially near the nominal $\upsilon = 1$ level.

separation between the HNO $\tilde{X}^1A'$ and $\tilde{a}^3A''$ states [ΔE_{s-t}(HNO)]. The latter is known from spectroscopy[13] to be 6275 ± 145 cm^{-1}, and subtracting this value from the $^3NO^-$ PA yields the dashed circle in Figure 4 (⊖). The correction places this isomer in remarkable agreement with the general trend. The energy of the ^{3}HON isomer relative to that of ^{3}HNO [denoted $\Delta E(^3\text{HNO} \rightarrow {}^3\text{HON})$] is not known experimentally, but on the basis of our CCSD(T) calculations, the ^{3}HON species lies about 1740 cm^{-1} higher in energy than ^{3}HNO. When the shift displayed by the OH_{IHB} of the O-bound isomer is corrected by this effective PA,

$$\text{PA}_{\text{eff}}(\text{O-bound}) = \text{PA}(^3\text{NO}^-) - \Delta E_{s-t}(\text{HNO}) - \Delta E(^3\text{HNO} \rightarrow {}^3\text{HON}) \quad (3)$$

(○ in Figure 4), the behavior is once again in excellent agreement with the shifts displayed by the other anions. This indicates that the CT interaction with the singlet proton-transfer pathway is negligible in $NO^-\cdot H_2O$ and that the differing shifts in the $O_2^-\cdot H_2O$ and $NO^-\cdot H_2O$ systems primarily reflect the relative proximities of the (spin-conserving) CT asymptotes. In particular, the larger shift displayed by $O_2^-\cdot H_2O$ can be definitively traced to increased CT resulting from the lower-lying proton-transfer pathway.

Having established the relative importance of the CT and electrostatic contributions, it is useful to consider how the CT interaction changes the shape of the potential governing the OH_{IHB} stretching motion. We explored this issue using complete-active-space SCF (CASSCF) calculations of the potential energy curves for proton transfer in $O_2^-\cdot H_2O$ and (N-bound) $NO^-\cdot H_2O$. These curves, reported in Figure 6, were generated by performing calculations for a series of O···H distances, R_1, optimizing all other degrees of freedom. From Figure 6, it is seen that the proton-transfer potential energy curve for the $O_2^-\cdot H_2O$ complex has a much more pronounced "flattening" at large R_1 values than does that of (N-bound) $NO^-\cdot H_2O$, the isomer that has the lowest proton-transfer asymptote. This is consistent with greater mixing with the CT configuration in the former case. Numerical solution of the eigenstates arising from the proton-transfer potential is difficult because of the correlated motion of the heavy atoms; therefore, we superimpose the harmonic energies of the $\upsilon = 0$ and 1 OH_{IHB} vibrational levels in Figure 6 to demonstrate the extreme nature of the anharmonicity on the scale of the first vibrational quantum. It is apparent that although part of the difference in red shifts between the OH_{IHB} bands of $O_2^-\cdot H_2O$ and $NO^-\cdot H_2O$ is recovered in the harmonic approximation a significant portion of the difference comes from anharmonicity effects, which are primarily manifested in the energy of the $\upsilon = 1$ level of $O_2^-\cdot H_2O$.

In summary, the OH stretching spectrum of the $NO^-\cdot H_2O$ complex is much simpler and less red-shifted than that of the related $O_2^-\cdot H_2O$ complex, although NO^- has the greater proton affinity. We trace this behavior to the lower effective proton affinity of the NO^- anion when electron spin is conserved in the intracluster proton-transfer reaction. This provides a dramatic qualitative illustration of how both electrostatic and charge-transfer effects are involved in the character of the anionic H-bond because both O_2^- and NO^- should display a similar electrostatic perturbation, whereas only O_2^- provides a spin-allowed, low-energy proton-transfer pathway. In comparing the behavior of the two systems, we conclude that over half of the red shift in the $O_2^-\cdot H_2O$ complex is due to CT-induced distortion of the potential function describing the H-bonded OH stretch.

Acknowledgment. This work was supported by the Experimental Physical Chemistry Division of the National Science Foundation and the U.S. Department of Energy under grant no. DE-FG02-00ER15066. Calculations were performed on computers in the University of Pittsburgh's Center for Molecular and Materials Simulations that were funded by NSF and IBM.

References and Notes

(1) Bailey, C. G.; Kim, J.; Dessent, C. E. H.; Johnson, M. A. *Chem. Phys. Lett.* **1997**, *269*, 122−127.
(2) Ayotte, P.; Weddle, G. H.; Kim, J.; Johnson, M. A. *J. Am. Chem. Soc.* **1998**, *120*, 12361−12362.
(3) Ayotte, P.; Weddle, G. H.; Kim, J.; Kelley, J. A.; Johnson, M. A. *J. Phys. Chem. A* **1999**, *103*, 443−447.
(4) Ayotte, P.; Kelley, J. A.; Nielsen, S. B.; Johnson, M. A. *Chem. Phys. Lett.* **2000**, *316*, 455−459.
(5) Kelley, J. A.; Weber, J. M.; Lisle, K. M.; Robertson, W. H.; Ayotte, P.; Johnson, M. A. *Chem. Phys. Lett.* **2000**, *327*, 1−6.
(6) Robertson, W. H.; Weddle, G. H.; Kelley, J. A.; Johnson, M. A. *J. Phys. Chem. A* **2002**, *106*, 1205−1209.
(7) Weber, J. M.; Kelley, J. A.; Nielsen, S. B.; Ayotte, P. A.; Johnson, M. A. *Science (Washington, D.C.)* **2000**, *287*, 2461−2463.
(8) Weber, J. M.; Kelley, J. A.; Robertson, W. H.; Johnson, M. A. *J. Chem. Phys.* **2001**, *114*, 2698−2706.
(9) Thompson, W. H.; Hynes, J. T. *J. Am. Chem. Soc.* **2000**, *122*, 6278−6286.
(10) *NIST Standard Reference Database Number 69*; NIST Chemistry WebBook; http://www.nist.gov (accessed 2002).
(11) Janaway, G. A.; Zhong, M. L.; Gatev, G. G.; Chabinyc, M. L.; Brauman, J. I. *J. Am. Chem. Soc.* **1997**, *119*, 11697.
(12) Janaway, G. A.; Brauman, J. I. *J. Phys. Chem. A* **2000**, *104*, 1795−1798.
(13) Ellis, H. B., Jr.; Ellison, G. B. *J. Chem. Phys.* **1983**, *78*, 6541−6558.
(14) Johnson, M. A.; Lineberger, W. C. *Techniques for the Study of Gas-Phase Ion Molecule Reactions*; Wiley: New York, 1988; p 591.
(15) Robertson, W. H.; Kelley, J. A.; Johnson, M. A. *Rev. Sci. Instrum.* **2000**, *71*, 4431−4433.
(16) Kendall, R. A.; Dunning, T. H., Jr.; Harrison, R. J. *J. Chem. Phys.* **1992**, *96*, 6796.
(17) Woon, D. E.; Dunning, T. H., Jr. *J. Chem. Phys.* **1993**, *98*, 1358.
(18) The calculations were performed using Gaussian 98, revision A.11. Frisch, M. J.; Trucks, G. W.; Schlegel, H. B.; Scuseria, G. E.; Robb, M. A.; Cheeseman, J. R.; Zakrzewski, V. G.; Montgomery, J. A., Jr.; Stratmann, R. E.; Burant, J. C.; Dapprich, S.; Millam, J. M.; Daniels, A. D.; Kudin, K. N.; Strain, M. C.; Farkas, O.; Tomasi, J.; Barone, V.; Cossi, M.; Cammi, R.; Mennucci, B.; Pomelli, C.; Adamo, C.; Clifford, S.; Ochterski, J.;

Petersson, G. A.; Ayala, P. Y.; Cui, Q.; Morokuma, K.; Malick, D. K.; Rabuck, A. D.; Raghavachari, K.; Foresman, J. B.; Cioslowski, J.; Ortiz, J. V.; Stefanov, B. B.; Liu, G.; Liashenko, A.; Piskorz, P.; Komaromi, I.; Gomperts, R.; Martin, R. L.; Fox, D. J.; Keith, T.; Al-Laham, M. A.; Peng, C. Y.; Nanayakkara, A.; Gonzalez, C.; Challacombe, M.; Gill, P. M. W.; Johnson, B. G.; Chen, W.; Wong, M. W.; Andres, J. L.; Head-Gordon, M.; Replogle, E. S.; Pople, J. A. *Gaussian 98*, revision A.11; Gaussian, Inc.: Pittsburgh, PA, 1998.

(19) Nielsen, S. B.; Ayotte, P.; Kelley, J. A.; Johnson, M. A. *J. Chem. Phys.* **1999**, *111*, 9563−9599.

(20) Corcelli, S. A.; Kelley, J. A.; Tully, J. C.; Johnson, M. A. *J. Phys. Chem.* **2002**, *106*, 4872−4879.

(21) de Beer, E.; Kim, E. H.; Neumark, D. M.; Gunion, R. F.; Lineberger, W. C. *J. Phys. Chem.* **1995**, *99*, 13627−13636.

(22) Yates, B. F.; Schaefer, H. F., III; Lee, T. J.; Rice, J. E. *J. Am. Chem. Soc.* **1988**, *110*, 6327−6332.

(23) Dixon, R. N. *J. Chem. Phys.* **1996**, *104*, 6905.

(24) Travers, M. J.; Cowles, D. C.; Ellison, G. B. *Chem. Phys. Lett.* **1989**, *164*, 449−455.

(25) Eaton, J. G.; Arnold, S. T.; Bowen, K. H. *Int. J. Mass. Spectrom.* **1990**, *102*, 303−312.

(26) Szmytkowski, C.; Maciag, K. *J. Phys. B: At. Mol. Opt. Phys.* **1991**, *24*, 4273−4279.

(27) Tennyson, J.; Noble, C. *J. Phys. B: At. Mol. Opt. Phys.* **1986**, *19*, 4025−4033.

(28) Solca, N.; Dopfer, O. *Chem. Phys. Lett.* **2001**, *342*, 191−199.